Bisphenol-Derived Single-Ion Conducting Multiblock Copolymers as Lithium Battery Electrolytes: Impact of the Bisphenol Building Block

Alexander Mayer, Alessandro Mariani, Xu Dong, Grégoire Vansse, Patrick Theato, Cristina Iojoiu, Stefano Passerini,* and Dominic Bresser*

ABSTRACT: Poly(arylene ether sulfone)-derived single-ion conducting (SIC) block copolymers are promising candidates as (solid) electrolytes for lithium-metal batteries owing to their high electrochemical stability and structural versatility. W hen incorporating small organic molecules (e.g., organic carbonates such as ethylene carbonate, EC), high ionic conductivities can be reached even at ambient temperatures. To gain further insights into the impact of the polymer backbone chemistry on the physicochemical and electrochemical properties, a series of SIC multiblock copolymers were synthesized comprising bisphenol-derived monomers for the ionophilic block. All of these SIC block copolymers (containing 55 wt % of EC) show high ionic conductivities. Remarkably, though, the electrochemical stability toward oxidation is slightly decreasing for an increasing size of the substituent at the central carbon atom of the bisphenol monomer, whereas the overpotential for lithium stripping and plating is decreasing. These results highlight the importance of carefully designing the polymer backbone for high-performance lithium battery electrolytes.

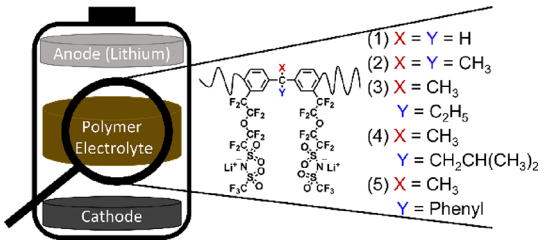

INTRODUCTION

Introduced to the mass market in the early 1990s,[1] lithium-ion batteries (LIBs) have nowadays captured almost every area of our daily life, spanning from portable electronic devices[2] to electric vehicles (EVs)[3] and even grid storage[4,5] for compensating the fluctuating renewable energy supply. This tremendous success is also the result of the great progress that has been achieved in optimizing LIBs toward higher energy and power densities.[6] However, to tackle the rising demand for future electrochemical energy storage, alternative battery technologies have to be evaluated, ideally providing even higher energy densities, faster charge process, and longer cycle life while simultaneously being cost-efficient, sustainable, and safe.[7,8] One of the most promising approaches toward higher-energy densities is the replacement of graphite and its composites with silicon[9] at the negative electrode by lithium metal owing to its exceptionally high capacity and very low redox potential.[10−12] Nonetheless, the standard liquid organic electrolytes commonly used in LIBs do not form a stable solid electrolyte interphase (SEI) on lithium metal electrodes, resulting in a continuous electrolyte decomposition, lithium loss, and in the worst case a highly inhomogeneous lithium deposition, eventually causing dendrite growth.[13−15]

Therefore, it is of utmost importance to identify viable alternative electrolyte systems, eventually enabling the transition from LIBs to lithium-metal batteries (LMBs). Up to now, the only commercial rechargeable LMB comprises an electrolyte based on poly(ethylene oxide) (PEO) and a conducting lithium salt.[16] Nonetheless, the need for elevated temperatures (about 60−80 °C) upon operation and charge owing to the strong coupling of charge transport and the segmental motion of the polymer, the limited stability toward potentials beyond 4 V, and the potential risk of Li^+ depletion at the electrodelelectrolyte interface have so far prevented the wide use of this technology in EVs.[16−22] The latter issue can be addressed by the use of single-ion conducting polymer electrolytes, where the negative charge is covalently tethered to the polymer backbone, inhibiting strong concentration gradients of the electroactive species in the electrolyte.[23−25] However, this commonly comes at the expense of lower conductivities not reaching the proposed target for EV applications of 4×10^{-4} S cm^{-1} for single-ion conducting electrolytes.[26]

In 2018, Nguyen et al.[27] presented an approach to overcome the conductivity issue by synthesizing a poly(arylene ether sulfone)-based single-ion conducting multiblock copolymer electrolyte via polycondensation and the subsequent introduction of small organic carbonate molecules (such as ethylene carbonate (EC) or propylene carbonate (PC)). These small molecules simultaneously act as plasticizer for the polymer and "molecular transporter" by coordinating the lithium ions and

thus facilitating the Li^+ conduction from one coordination site to another.[27] In such single-ion conducting block copolymer electrolytes (SIC-BCEs), the ionophilic block, comprising the lithiated side chains attached to the polymer backbone, enables the charge transport. The ionophobic block, instead, guarantees the mechanical stability and self-standing properties of the polymer membrane even after swelling with the small organic carbonate molecules. Remarkably, the electrochemical stability window of this system allowed for stable long-term lithium stripping and plating even at elevated current densities, as well as the successful cycling of Li|SIC-BCE|NMC_{811}[28] and Li|SIC-BCE|NMC_{622}[29] cells at ambient temperature. Targeting a better understanding of the chemistry of the polymer backbone, we investigated very recently the influence of a fluorinated polymer backbone[30] and the replacement of the ether function by a thioether function.[31] The latter revealed a reduced electrochemical stability toward oxidation, whereas the former led to an enhanced electrochemical stability accompanied by a stabilized interface with lithium-metal electrodes resulting from a fluorine-richer interphase.

Herein, we extended our study on the impact of the backbone design on the electrochemical properties of the resulting electrolytes by replacing the biphenyl monomer by different bisphenol derivatives. This exchange enables the investigation of a comprehensive set of molecular building blocks in the ionophilic part of the block copolymer while maintaining all residual contributions. The results show that even relatively minor changes influence the electrochemical stability and, especially, the overpotential in lithium stripping/plating experiments.

EXPERIMENTAL SECTION

Synthesis of the Bisphenol-Containing Polymer Backbone.

The synthesis of the bisphenol-containing polymer electrolyte was performed according to previous studies[27,32,33] with some minor modifications. In brief, the polymerization of the multiblock copolymer backbone is performed in a one-pot-two-step reaction, adjusting the 2:1 ratio of the ionophilic and ionophobic block. This is followed by the bromination of the ionophilic blocks and the subsequent substitution of these brominated reactive sites by the lithiated side chains via a copper-catalyzed Ullmann-type coupling reaction. A detailed description of the synthesis and the intermediate products is provided in the Supporting Information (see Figure S1 and Table S1−S3). The synthesis of the lithium-containing side chain (I-psiLi) was performed following a previously reported synthesis route.[27]

Membrane Fabrication and Swelling with Ethylene Carbonate. Polymer membranes were prepared via solvent casting by dissolving 1 g of the polymer electrolyte powder in 10 mL of DMSO (1:10 w/v) on a roll mixer at room temperature. Subsequently, the solution was subjected to centrifugation (30 min, 6000 rpm) to remove any solid impurities and air bubbles. The transparent brownish solution was then poured into a Petri dish (ca. 11 cm in diameter), which was covered with a perforated aluminum foil to slowly evaporate the solvent at 70 °C. The procedure yielded thin polymer films of around 50 μm (±10 μm). The polymer membranes were further dried *in vacuo* at 150 °C for 24 h and immersed in demineralized H_2O for 48 h to evaporate and dissolve residual traces of the solvent. Round discs (18 mm in diameter) were punched out and dried at 130 °C, sandwiched between two Petri dishes for 24 h. The resulting membranes were stored in a dry room atmosphere (dew point < −65 °C). Finally, polymer electrolyte membranes swollen with EC were fabricated by immersing the polymer membrane in molten EC on a hot plate at 45 °C (50 °C for BP-F). The EC content was adjusted by using the desired amount of EC and a surplus of ca. 5 wt % (e.g., for 55 wt %, EC for 60 wt % was provided on a Teflon Petri dish on the hot plate). An additional annealing step in a climatic chamber (Binder KB23) at 40 °C for at least 24 h was performed to warrant the homogeneous distribution of EC in the polymer membrane. The solvent content (SC, wt %) was calculated using eq 1, and the weight of the dry (W_d) and the swollen membranes (W_s) was 55 wt % (±1 wt %), if not stated otherwise:

$$SC = \frac{W_s - W_d}{W_s} \times 100\% \quad (1)$$

It appears noteworthy that the addition of EC to BP-A/B/DMB/AP mainly translated into an increased thickness (basically doubled for 55 wt % EC) of the polymer membrane while maintaining a diameter of ca. 18 mm. Differently, for BP-F, essentially an in-plane expansion of the polymer membrane to approximately 22 mm diameter (+50% in area) was observed, with only a minor increase in thickness.

Physicochemical Characterization. The synthesized polymers and intermediate products were characterized by ^1H and ^{19}F nuclear magnetic resonance (NMR) spectroscopy complemented by ^{13}C and 2D NMR experiments ($^1H,^1H$-COSY, $^1H,^{13}C$-HSQC, and $^1H,^{13}C$-HMBC) on a Bruker Ascend 400 MHz using the untreated polymer backbone of BP-F as an example. The molecular mass distribution was determined by gel permeation chromatography (GPC, Malvern Panalytical OmniSEC multidetector system) using 0.05 M LiBr in DMF as the eluent (further details are provided in the Supporting Information). Differential scanning calorimetry (DSC, Discovery series, TA Instruments) was performed with a heating rate of 5 K min^{-1} (sample size: ∼10 mg in sealed aluminum pans, −100 to 230 °C or −100 to 100 °C, N_2 gas flow: 10 mL min^{-1}). The second heating cycle was used for the data evaluation. Thermogravimetric analysis (TGA, Netzsch TG 209 F1) was carried out with a heating rate of 5 K min^{-1} in sealed aluminum pans (with a small hole punched in the cap prior to the measurement as a gas exhaust) between 30 and 600 °C under synthetic air (N_2/O_2 80:20 v/v) using a sample mass of approximately 2 mg. The ion-exchange capacity (IEC) was measured by acid−base titration in an organic solvent. The titrant solution was prepared by dissolving 0.05 g of anhydrous NaOH in 100 mL of diethylene glycol monoethyl ether (DGME). The analyte solution was prepared by dissolving 0.1 g of ionomer powder in the acidic form in 5 mL of DGME. The acidic form of the ionomer was obtained by stirring the powder in a 2 M HCl solution for 24 h; the powder was then dried at 60 °C *in vacuo* for 12 h. Methyl orange was used as a pH indicator for the titration.

Electrochemical Characterization. The determination of the ionic conductivity was performed in symmetric Cu|Cu cells at varying temperatures. The polymer electrolyte membranes were sandwiched between two battery-grade copper foils in pouch cells. The cell assembly was performed in a dry room (dew point < −65 °C). After sealing the pouch cells using a vacuum sealer (Audiovac VMS 163, Audion), they were stored at 40 °C for at least 24 h prior to the measurements to allow for the homogenization of the interfaces. Electrochemical impedance spectroscopy (EIS) was performed using a Solartron SI 1260/1287 Impedance Analyzer in the frequency range from 1 Hz to 1 MHz. The measurements were performed at different temperatures using a Binder climatic chamber with a 3 h rest period at each temperature upon cooling and heating. The subsequent data analysis was carried out with the RelaxIS 3 software (rhd instruments), and the resistance R was determined by applying an *RP* fitting model. The ionic conductivity (σ) was determined via eq 2, considering the thickness d of the polymer membrane (determined with a Mitutoyo absolute digital thickness gauge 547-401) and the area A of the polymer membrane covered by both copper electrodes:

$$\sigma = \frac{d}{RA} \quad (2)$$

Lithium stripping/plating experiments were conducted in coin cells (CR2032, Hohsen) at 40 °C (Binder climatic chamber) using a Maccor 4000 battery testing system. Disk-shaped lithium foils (14 mm in diameter, 500 μm thickness, battery grade, Honjo) were placed

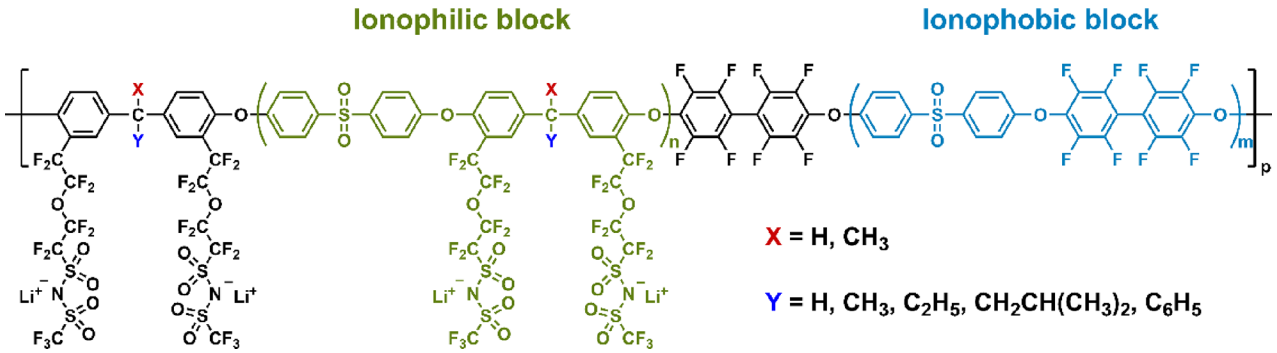

Figure 1. General structure of the bisphenol-containing single-ion conducting multiblock copolymer electrolytes with a block ratio of 2:1 (ratio of the ionophilic block compared to the ionophobic block). The conductive ionophilic block carries the lithiated side chains, and the partially fluorinated ionophobic block provides mechanical stability.

Table 1. Chemical Structure, Substitution Pattern, and Systematic and Trivial Names of All Bisphenol Monomers Studied in This Work[a]

Structure / Color	X / Y =	Systematic Name	Trivial Name	Short
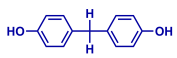	X = Y = H	4,4'-methylene diphenol	bisphenol F	BP-F
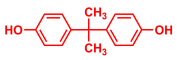	X = Y = CH_3	4,4'-isopropylidene diphenol	bisphenol A	BP-A
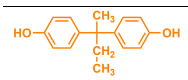	X = CH_3 Y = C_2H_5	4,4'-(1-methyl propylidene)diphenol	bisphenol B	BP-B
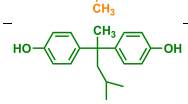	X = CH_3 Y = $CH_2CH(CH_3)_2$	4,4'-(1,3-dimethyl butylidene)diphenol	bisphenol DMB	BP-DMB
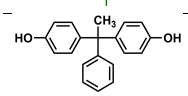	X = CH_3 Y = C_6H_5	4,4'-(1-phenyl ethylidene)diphenol	bisphenol AP	BP-AP

[a]To simplify the identification of the respective monomer and the resulting polymer, abbreviations and colors are used, as displayed in the table.

on spacers made of stainless steel (16 mm, 0.5 mm thickness) followed by sandwiching the EC-doped polymer membranes (90 ± 10 μm thickness, 60 ± 10 μm for BP-F) between the lithium disks in an argon-filled glovebox (MBRAUN MB-200-MOD, H_2O/O_2 < 1 ppm). The coin cells were sealed using a hydraulic coin cell crimping machine (MSK-110, MTI Corp., pressure of ~800 psi). The current density was gradually varied from 5 to 10, 20, 50, 100, and 200 μA cm^{-2}, and the current was reversed after 1 h, intermitted by a 5 min rest step. Long-term stripping and plating experiments were performed at a current density of 100 μA cm^{-2} and stopped after a short circuit was observed or when the cell reached 1000 h of continuous cycling.

The electrochemical stability window was determined via linear sweep voltammetry (LSV). For this purpose, two-electrode pouch cells with nickel foil as the working electrode and lithium foil (50 μm thickness, battery grade, Honjo) as the counter electrode were assembled in a dry room (dew point < −65 °C). The measurements were performed with a BioLogic VMP3 Multichannel Potentiostat at 40 °C (Binder climatic chamber KB23) at a sweep rate of 1 mV s^{-1} after a rest time of 24 h. The cutoff voltages were set to −2.0 and +6.0 V. Freshly assembled cells were used for each LSV experiment.

The Li^+ transference number t_{Li^+} was determined using the "polarization method" developed by Bruce, Vincent, and Evans in 1987.[34] To perform the experiment, a symmetric Li|Li coin cell was assembled and placed in a climatic chamber (Binder) at 40 °C for 48 h to ensure thermal equilibrium. The cell was then polarized with 10 mV, and the current was measured until a steady state was achieved. An impedance analyzer (Solartron SI 1260/1287) with a frequency range of 1 Hz to 1 MHz was used to perform impedance measurements before and after polarization, and the RelaxIS 3 software (rhd instruments) was used to analyze the data. The transference number t_{Li^+} was calculated using eq 3, which involves I_0 and I_{ss} (current measured right after polarization and at steady state, respectively), R_0 and R_{ss} (resistance before polarization and at steady state, respectively, measured by electrochemical impedance spectroscopy (EIS)), and the polarization applied to the cell (ΔV). This calculation was done following the recommendations reported earlier.[35,36]

$$t_{Li^+} = \frac{I_{ss}(\Delta V - I_0 R_0)}{I_0(\Delta V - I_{ss} R_{ss})} \quad (3)$$

DFT Calculations. DFT calculations were performed with Gaussian16[37] at the B3LYP/6-311++G** level of theory. The starting guess geometries were hand-drawn using Avogadro[38] and then optimized using ultrafine thresholds. The Gibbs free energies were obtained by performing a frequency calculation on the obtained configurations, including the thermal (298 K) and zero-point-energy contributions. No imaginary frequency was observed for the optimization step, confirming the obtained geometry as a minimum of the potential energy surface. The effect of the solvation shell was included by means of a polarizable continuum model (PCM) using the static and dynamic dielectric constants of pure EC (95.3 and 2.005). The geometries obtained from the optimization of the singlet states (i.e., the neutral ethers) were then used as starting configurations for the two doublet states, where a single electron was either injected (reduction) or removed (oxidation) from the system. The energy values of the doublet states were obtained by single point calculations because the electron exchange is much faster

than the nuclear rearrangement. The Nernst−Einstein relationship then provided the absolute redox potentials, which were converted in potentials vs Li^+/Li by adding and subtracting 1.38 ± 0.2 V (considering 4.6 ± 0.2 V for the standard hydrogen electrode[39,40] and −3.04 V for the Li^+/Li redox couple) for the reduction and oxidation, respectively. A complete overview on the methodology can be found elsewhere.[41,42] In summary, the following equations were used:

$$\Delta G_{298}^{\mathrm{RedOx}} = G_{298}^{\mathrm{Ox}} - G_{298}^{\mathrm{Red}} \tag{4}$$

$$V_{\mathrm{Abs}} = \frac{\Delta G_{298}^{\mathrm{RedOx}}}{n \cdot F} \tag{5}$$

$$V_{\mathrm{vs.Li}} = V_{\mathrm{Abs}} + (V_{\mathrm{Abs}}^{\mathrm{SHE}} + V_{\mathrm{Li^+/Li}}) \tag{6}$$

where $\Delta G_{298}^{\mathrm{RedOx}}$ is the reduction free energy difference at 298 K; G_{298}^{Ox} and G_{298}^{Red} are the Gibbs free energy of the oxidized and reduced states, respectively; V_{Abs} is the absolute reduction potential; n is the number of exchanged electrons; F is the Faraday constant; $V_{\mathrm{Li^+/Li}}$ is the standard reduction potential of the Li^+/Li redox couple; $V_{\mathrm{Abs}}^{\mathrm{SHE}}$ is the absolute potential of the standard hydrogen electrode; and $V_{\mathrm{vs.\ Li}}$ is the reduction potential vs the Li^+/Li redox couple. Energy terms are expressed in kJ mol^{-1}, potential values are expressed in V, and the Faraday constant is 96.485 kC mol^{-1}.

RESULTS AND DISCUSSION

The general structure of the bisphenol-containing ionomers investigated in this work is presented in Figure 1. To allow for the facile identification of all different bisphenol derivatives and the resulting SIC-BCEs, Table 1 shows the color and abbreviation used to distinguish the respective materials in the subsequent figures, their chemical structure, the systematic and trivial names, as well as the substituents at the central carbon atom. It may be noted that bisphenols are commercially well established as monomers for the synthesis of polycarbonates and epoxy resins,[43] thus providing the chance to serve as affordable and highly abundant educts for the synthesis of polymer electrolytes. Nonetheless, it should also be mentioned that bisphenols have been classified as hazardous substances because they act as xenoestrogens and endocrine disruptors in the human body,[43,44] which are especially critical in the case of a lifelong exposure to trace amounts of these species.[45,46] When comprised in closed battery cells though, this might be less of an issue, as the potential exposure to the environment is limited (depending also on the eventual recycling). In either case, the bisphenols serve as very good model compounds for the comprehensive investigation of different chemical motifs in the polymer backbone and their impact on the physicochemical and electrochemical properties of the resulting SIC-BCEs.

Generally, the ^1H NMR spectra of the first block (later becoming the ionophilic block) showed the expected signals, and the ^{19}F NMR spectra showed no or only very minor traces of unreacted monomer (see Figures S2, S6, S8, S10, and S12). The ^1H and ^{19}F NMR spectra of the final polymer backbone (see Figures S3, S7, S9, S11, and S13) also showed the expected signals and confirmed the targeted 2:1 ratio of the ionophilic and ionophobic block. To allow for the unambiguous identification and allocation of all NMR signals to the polymer structure, ^{13}C NMR and 2D NMR experiments ($^1H,^1H$-COSY, $^1H,^{13}C$-HSQC, and $^1H,^{13}C$-HMBC) were performed exemplarily for the BP-F polymer (see Figures S4 and S5). All anticipated signals and couplings were detected, except the carbon signals of the perfluorinated monomer in the ionophobic block (C_{14}−C_{17}, Figure S4 top), owing to the strong carbon−fluorine coupling and the resulting low signal intensity of strongly splitting multiplets. However, the ^{19}F spectra clearly prove the incorporation of this monomer in the polymer backbone. Furthermore, the successful polymerization of all monomers is highlighted by the GPC data provided in Table S4. For the first step of the polymerization, the reaction time and temperature were constant. The dispersity ($Đ = M_w/M_n$) of the first block was still significantly below the theoretical value of 2, indicating an incomplete conversion, as desirable for the formation of multiblock copolymers. In the second step of the polymerization, where the polymer backbone is completed with the ionophobic block, both parameters were adjusted to the respective monomer (higher reaction time and temperature with the increasing bulkiness of the substituent at the central C atom; see also Table S2 for further details). This allowed for the synthesis of polymers exhibiting relatively similar molecular masses and, thus, better comparability. $Đ$ was slightly higher than 2, most likely due to the complex structure of these multiblock copolymers (e.g., branching at the decafluorobiphenyl monomer due to the reactivity of fluorine substituents in ortho and meta position[33,47]) resulting in nonideal polymerization conditions and a potentially slight stoichiometric imbalance of the monomers.

The subsequent bromination of the polymer backbones with elemental Br_2 resulted in the formation of a dibrominated polymer chain without any noticeable side products in the case of BP-A, BP-B, BP-DMP, and BP-AP (see the NMR spectra displayed in Figures S15−S18). Interestingly, the ^1H NMR spectrum of BP-F (Figure S14) indicated that the bromination was not limited to the phenyl rings but also occurred at the central carbon atom with a ratio of about 80:20 (Figure S14; H_4', H_5', and H_8'). This was somewhat unexpected (at least in this rather high ratio) because the substitution at the central carbon atom (i.e., the "side chain" of the aromatic system, if any) is usually associated with high temperatures and/or light irradiation,[48−50] whereas low temperatures favor the substitution at the aromatic ring. However, because the central carbon atom is stabilized by two phenyl rings, benzylic bromination via a radical mechanism might occur. Compared to the nonbrominated polymer backbone, a minor decrease of about 10% in the molar ratio of the ionophilic and ionophobic block was apparent from the integrals of *inter alia* the two protons exhibiting the highest downfield shift in the ^1H NMR spectra of the brominated polymers (H_2 and H_7 (BP-F and BP-A)/H_9 (BP-B)/H_{10} (BP-DMB/BP-AP), somewhat more with almost 20% in the case of BP-AP). Additionally, GPC measurements (Table S4 and Figure S24) showed a slight decrease in molecular mass after the bromination. This can be due to a different solvent interaction resulting in different elution times, which translates into lower masses when calculated based on PMMA calibration standards, or in a chain cleavage, enabling the dissolution of such shorter fragments in methanol. Remarkably, BP-AP does not follow this trend, and the brominated polymer exhibits a higher molecular mass compared to the educt, suggesting either that the bulky phenyl substituents effectively protect the polymer from chain cleavage under these reaction conditions or that these bulky phenyl substituents after bromination result in better solvent interaction and thus an earlier elution. Eventually, the lithiated side chain was coupled to the polymer backbone via a copper-catalyzed Ullmann reaction, as confirmed by NMR spectroscopy (Figures S19−S23) and a substantial increase in molecular mass (Table S4). It is

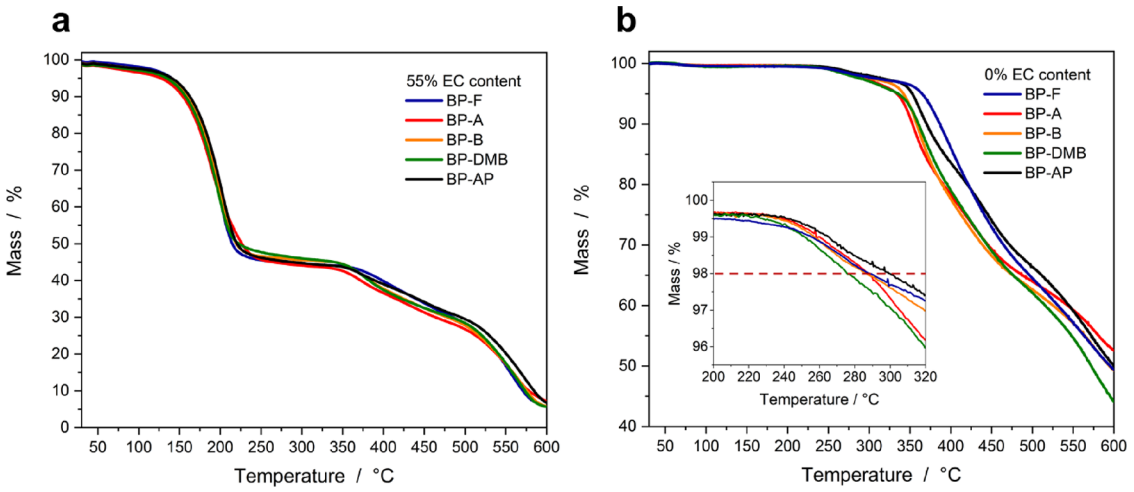

Figure 2. (a) TGA curves of the various SIC-BCEs comprising 55 wt % EC. (b) TGA curves of the dry ionomers. The inset provides a magnification of the region between 200 and 320 °C, highlighting the onset temperatures of the thermal decomposition, defined herein as a mass loss of 2 wt %.

Table 2. Summary of the Characteristic Thermal and Electrochemical Properties of the Bisphenol-Based SIC-BCEs: (1) Onset Temperature of the Thermal Decomposition of the Dry Ionomers; (2) Glass Transition Temperature of the Ionophilic Block of the SIC-BCEs Comprising 55 wt % EC; (3) Ionic Conductivity at 40 °C (55 wt % EC); (4 and 5) Oxidative Stability of the Electrolyte Membranes Containing 55 wt % EC When Applying a Current Density Limit of 10 and 5 μA cm^{-2}

Ionomer	Decomposition onset (dry) / °C	T_g ionophilic block (55 wt.-% EC) / °C	Ionic conductivity (55 wt.-% EC, 40 °C) / mS cm^{-1}	Oxidative stability (10 µA cm^{-2}) / V	Oxidative stability (5 µA cm^{-2}) / V
BP-F	289	-80	0.52	4.74	4.55
BP-A	288	-82	0.55	4.68	4.56
BP-B	287	-86	0.51	4.59	4.47
BP-DMB	276	-85	0.56	4.62	4.48
BP-AP	300	-84	0.35	4.56	4.39

noteworthy that BP-F also does not show any side products in the ^{19}F NMR spectrum, confirming that the coupling of the side chain remained limited to the active sites at the phenyl rings. The determination of the ion-exchange capacity (IEC) generally revealed a decreasing IEC for an increasing size of the substituent at the central carbon atom due to the larger influence of the substituent on the overall molecular weight and, therefore, Li^+ concentration (Table S5).

Following the successful synthesis of all bisphenol-based SIC-BCEs, membranes were prepared for each of them and swollen with 55 wt % EC. The content of the latter was confirmed by TGA along with the determination of the thermal stability of such ionomers (Figure 2). As observed in Figure 2a, the evaporation of EC started at around 140 °C and was completed at 300 °C, as indicated by a small plateau and the mass loss of about 55 wt %. Subsequently, the thermal decomposition of the ionomer sets in. This has been further studied by performing TGA for the dry ionomer membranes (Figure 2b). For a comparison of the different bisphenol-based ionomers, the decomposition temperature was defined herein as a mass loss of 2% (see the inset Figure 2b). The results are summarized in Table 2. This comparison revealed that the relatively "simple" ionomers BP-F, BP-A, and BP-B exhibited very similar decomposition temperatures of around 290 °C. For BP-DMB, comprising a longer alkyl chain substituent, a reduced thermal stability of ca. 275 °C was detected, suggesting that the longer alkyl chain favored the temperature-induced decomposition. Differently, the phenyl substituent in BP-AP appeared to stabilize the ionomer toward elevated temperatures, and the thermal stability was increased to about 300 °C. A comparison with the biphenyl-based SIC-BCEs reported earlier, which showed a thermal stability of more than 300 °C,[27,30] indicated that the replacement of the biphenyl unit by the bisphenol derivatives generally led to a moderate drop in thermal stability owing to the additional cleaving sites introduced into the polymer backbone.

The influence of the now spatially separated aromatic systems in the bisphenol-containing polymer backbone was further unraveled by DSC measurements (Figure S25). Compared to the earlier reported ionomers comprising

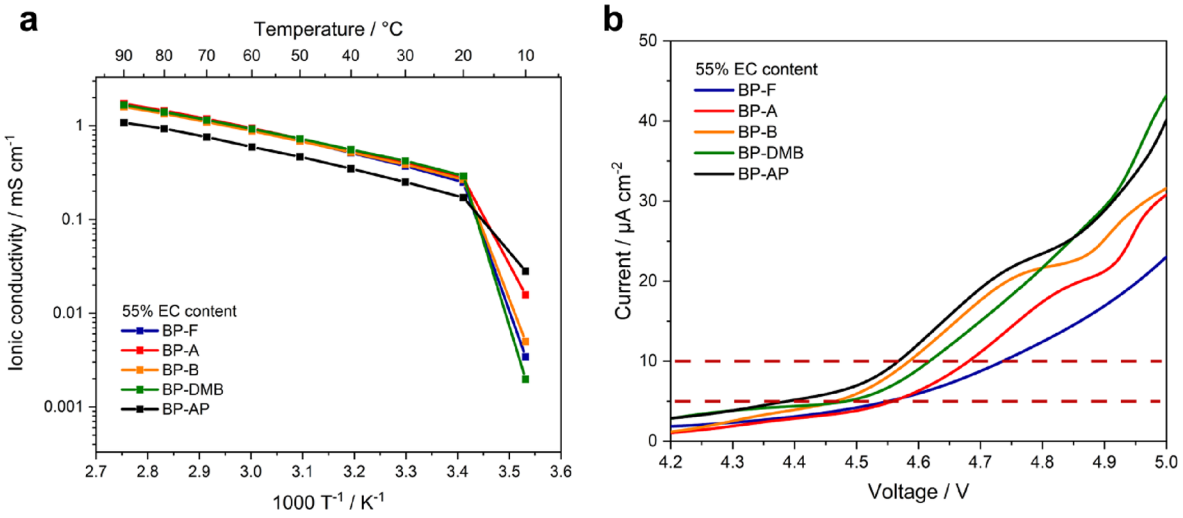

Figure 3. (a) Comparison of the ionic conductivity of the different SIC-BCEs at varying temperatures and a fixed EC content of 55 wt %. (b) Superimposed LSV traces of the oxidative sweeps recorded for the SIC-BCEs; the dashed horizontal lines indicate the current density limits of 10 and 5 μA cm^{-2} that were used for the determination of the electrochemical stability toward oxidation.

biphenyl moieties, which showed a T_g of the ionophilic block of around −40 °C at 55 wt % EC,[27] the bisphenol-containing ionomers were characterized by a substantially lower T_g of the ionophilic block of −80 °C and less. This decrease in T_g is assigned to the more flexible bisphenol polymer backbone. Among the bisphenol derivatives, a slight trend toward lower T_g values was observed for an increasing size of the substituent at the central carbon atom (Table 2). This trend is attributed to the increasing bulkiness of such substituents, providing additional free volume and, therefore, flexibility to the polymer chains. The T_g of the ionophobic block, however, remained the same as found earlier for the biphenyl-comprising ionomers[27,30,31] with about 220 °C. Moreover, the T_g remained unaffected by the incorporation of EC, as exemplarily shown for BP-A in Figure S26a, evidencing the preferred coordination of the EC molecules in the ionophilic domains. Figure S26b reveals another remarkable effect, i.e., the absence of any EC melting peak for an EC content below 50 wt %. This finding underlines the strong coordination of the EC molecules by the ionophilic block, which is in excellent agreement with the previous studies on biphenyl-based SIC-BCEs.[27,30,31]

When the EC content is increased to 50 wt % and more, domains of free EC molecules are formed, and the crystallization of these domains becomes more and more pronounced. In addition, no EC crystallization signal was found in the cooling cycles prior to the second heating cycles used for the data evaluation for the different bisphenol ionomers (Figure S25 bottom right) or the different EC contents of BP-A (Figure S26c). Only for the highest EC content of 60 wt % did a minor signal become apparent. The EC melting enthalpies of all bisphenol ionomers at 55 wt % EC and at different EC contents using the BP-A ionomer are summarized in Table S6. By dividing these values through the enthalpy of fusion of EC, the content of free EC molecules was estimated. Whereas it was as low as 5% for an EC content of 50 wt %, the value increased to around 25% for 55 wt % EC and approximately 30% free EC for an EC content of 60 wt %.

Subsequently, the impact of the EC content on the ionic conductivity was studied as well, and the results are displayed in Figure S27. Generally, the conductivity increased with an increasing EC content, as expected. For an EC content of 50 wt % and more, however, the conductivity sharply dropped at 20 °C and below (depending on the EC content), which has been assigned to the crystallization of the free EC domains, blocking the charge transport pathways in the membranes.[27,30,31]

More important for the present study was the direct comparison of the different bisphenol-containing SIC-BCEs, which is exemplarily depicted in Figure 3a for an EC content of 55 wt %. It appeared that the choice of the bisphenol building block did not have a significant impact on the ionic conductivity for this EC content, except for BP-AP, which showed a slightly lower conductivity. This can be probably ascribed to the bulky phenyl group, which might hamper the mobility of the ionic side chains and the inter-side-chain Li^+ transport. In addition, it is noteworthy that the substantially lower T_g of the ionophilic block compared to the biphenyl-based SIC-BCEs reported earlier[27] (i.e., about −80 °C vs −40 °C) appears to have only a minor effect on the ionic conductivity, as it showed only a moderate increase from around 0.4−0.5 mS cm^{-1} to about 0.5−0.6 mS cm^{-1} (see Table 2) at the same EC content and temperature, although the different ionomer chemistry and/or the block ratio might also play a role. This finding confirmed that the charge transport in these electrolyte systems was (at least) partially decoupled from the segmental dynamics of the polymer backbone and is largely supported by the EC molecules coordinating the lithium cations, resulting in a more vehicular-type charge transport and lowering the activation energy needed for the "hopping" from one anionic site to another.[16] Such mechanism is different from the charge transport in classic dry PEO-based electrolytes[51,52] and dry SIC-BCEs such as P(STFSILi)-*b*-PEO-*b*-P(STFSILi),[53] in which the lithium cation is coordinated by the ether functions of PEO (or the PEO block) and, thus, solely/highly dependent on the segmental dynamics of the PEO (block), in addition to the dissociation from the counterion. To confirm the nevertheless single-ion conducting behavior of the bisphenol-based ionomers, the Li^+ transference number t_{Li^+} was determined via the Bruce−Vincent−Evans method. All values obtained are found to be very close to unity, i.e., in the range of 0.95−0.98 (Table S7 and Figure S28), and minor differences might

originate from the presence of polarizable short molecules such as oligomeric structures or the spontaneous reactions occurring at the interface with the lithium-metal electrodes.[54]

In a next step, the impact of the bisphenol building block on the electrochemical stability was investigated by LSV (Figure S29). Generally, all SIC-BCEs showed a very comparable behavior with two broad reductive peaks at about 1.05−1.15 and 0.3−0.35 V, which have been assigned to the initial decomposition of minor traces of the casting solvent DMSO[55] and EC,[56] respectively. Below 0 V, the plating of metallic lithium on the working electrode was observed. The oxidative decomposition of the polymer electrolytes was observed at more than 4.5 V vs Li^+/Li, as indicated by the sharply rising currents. A direct comparison of all SIC-BCEs in this voltage range is provided in Figure 3b. Interestingly, the bulkier the substituent is, the lower is the electrochemical stability toward oxidation even though the difference between the most (BP-F) and least (BP-AP) stable SIC-BCE is only about 0.2 V (depending also on the current limit chosen for the determination of the stability; see Table 2). Presumably, the bulkier substituents, specifically the aromatic benzyl group, stabilized the oxidation decomposition products. The latter eventually approach the electrochemical stability of biphenyl-based ionomers.[27] These findings add another cornerstone to the understanding of poly(arylene ether sulfone)-based ionomers and complement previous results of our group on the reduced electrochemical stability for a nonfluorinated backbone and a thioether-containing ionomer.[30,31]

To corroborate these experimental findings, we conducted DFT calculations for BP-F, BP-A, BP-B, BP-DMB, and BP-AP, i.e., the different ionophilic blocks, which were simplified by removing the lithiated side chain (as these are chemically the same for all SIC-BCEs) to reduce the computational effort. The results are summarized in Table 3 (see also Table S8 for additional details). The given stability limits were calculated for an EC environment to reflect the experimental environment, and in fact, the results are in very good agreement with the experimental findings. The larger the substituent was, the lower was the electrochemical stability toward oxidation, whereas the stability toward reduction appeared to be not affected and well within the lithium plating regime below 0 V.

Table 3. Enthalpy Thresholds for the Reduction/Oxidation and the Resulting Electrochemical Stability Window vs Li^+/Li of the Simplified Repeating Unit of the Ionophilic Block of the BP-F, BP-A, BP-B, BP-DMB, and BP-AP SIC-BCEs as Determined by DFT Calculations[a]

	Stability vs. Reduction		Stability vs. Oxidation	
	ΔG / kJ mol^{-1}	Voltage vs. Li^+/Li	ΔG / kJ mol^{-1}	Voltage vs. Li^+/Li
BP-F	180.4	-0.3 ± 0.2	620.0	4.9 ± 0.2
BP-A	178.0	-0.3 ± 0.2	603.9	4.7 ± 0.2
BP-B	177.9	-0.3 ± 0.2	588.9	4.5 ± 0.2
BP-DMB	180.8	-0.3 ± 0.2	585.2	4.5 ± 0.2
BP-AP	177.8	-0.3 ± 0.2	572.7	4.4 ± 0.2

[a]The rather large error range of ±0.2 V originates from the inherent error of the standard hydrogen electrode[39,40] when converting the results of the DFT calculations into electrochemical stability values vs Li^+/Li.

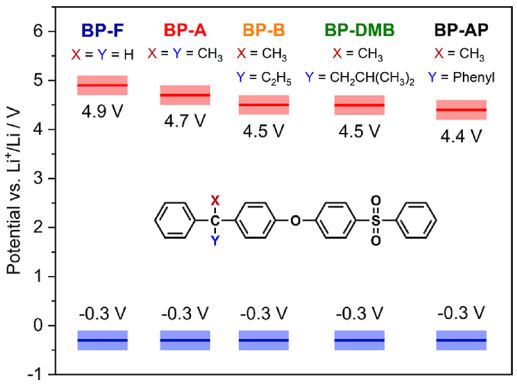

Figure 4. Graphical representation of the electrochemical stability window for the simplified ionophilic block of BP-F, BP-A, BP-B, BP-DMB, and BP-AP as determined by DFT calculations, including the error range.

Figure 4 once more highlights these findings by presenting a graphical illustration of the different electrochemical stability windows as a function of the substituents, along with the chemical structure of the simplified model compounds used for the calculations.

Finally, the compatibility with lithium-metal electrodes was further studied by assembling symmetric Li|SIC-BCE|Li cells and subjecting them to galvanostatic lithium stripping and plating experiments. The overpotential as a function of the applied current density is depicted in Figure 5, and the corresponding values are provided in Table S9. Remarkably, BP-F and BP-A showed a substantially higher overpotential (essentially doubled) compared to the other three SIC-BCEs with bulkier substituents, suggesting a more favorable interface and, presumably, interphase with the lithium-metal electrodes that allowed for a facilitated charge transfer.

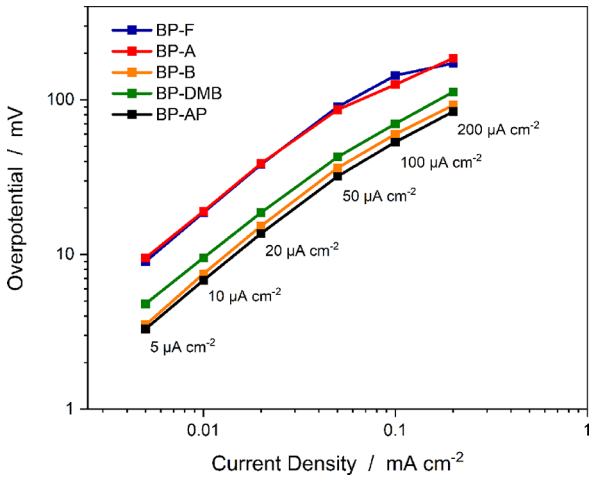

Figure 5. Overpotential vs current density derived from the lithium stripping and plating experiments for all bisphenol-based SIC-BCEs comprising 55 wt % EC at 40 °C.

This trend is further corroborated by long-term stripping and plating experiments at a constant current density of 100 μA cm^{-2} (Figure 6). The cells comprising BP-F and BP-A showed a relatively high overpotential and a (soft) short circuit

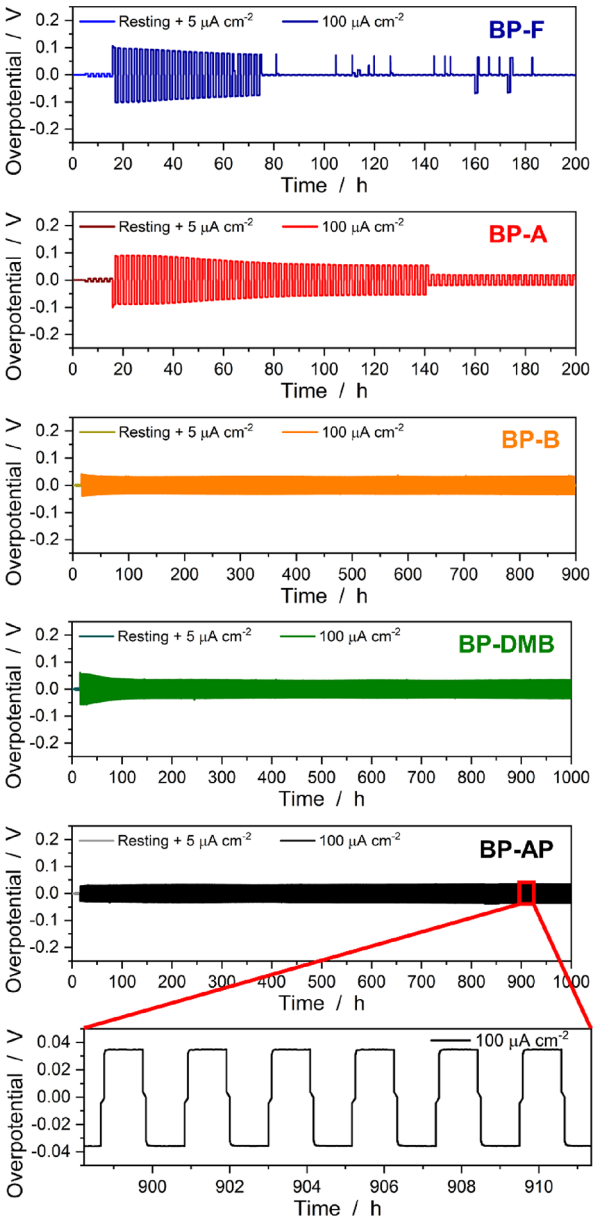

Figure 6. Comparison of the long-term galvanostatic lithium stripping and plating in symmetric Li|SIC-BCE|Li cells at a current density of 100 μA cm^{-2} for the different bisphenol-based ionomers (T = 40 °C). At the bottom, a magnification of the lithium stripping and plating cycles of the Li|BP-AP|Li cell after about 900 h is shown, as also indicated by the red square in the upper plot.

after less than 100 and 200 h, respectively. For the BP-F, these can be attributed to the acidic protons in the methylene group bridging the two aromatic rings. Differently, BP-B, BP-DMB, and BP-AP exhibited a substantially lower (and among each other comparable) overpotential—though still higher than ionomers comprising a biphenyl instead of a bisphenol moiety[27,30]—with a greatly improved cycle life of up to 1000 h and without any significant increase in overpotential, in fact, and the expected essentially constant voltage response for a single-ion conducting polymer-based electrolyte, as exemplarily shown for BP-AB.

CONCLUSIONS

The successful synthesis of five different single-ion conducting multiblock copolymer electrolytes based on a polymer backbone comprising different bisphenol derivatives has been reported. The direct comparison of the electrochemical properties revealed that:

- Very bulky substituents, as represented herein by a phenyl group, lead to a slightly lower ionic conductivity (0.35 vs about 0.55 mS cm^{-1} at 40 °C and 55 wt % EC).
- The larger the substituent is, the lower is the electrochemical stability toward oxidation, which is ascribed to the formation of thermodynamically stabilized electrochemical decomposition products.
- The larger the substituent is, however, the lower is the overpotential upon lithium stripping and plating and the better is the cycling stability, indicating a favorable interface with lithium-metal electrodes and the formation of a more stable interphase, which suppresses short-circuiting of the cells.

Generally, we may anticipate that the careful modification of the bisphenol building block and the resulting fundamental insights into the impact of the chemical structure of this building block will help to develop further optimized (single-ion conducting) polymer electrolytes with superior electrochemical performance—benefitting from both high stability toward oxidation and suitable compatibility with lithium-metal electrodes.

AUTHOR INFORMATION

Corresponding Authors

Stefano Passerini − *Helmholtz Institute Ulm (HIU), 89081 Ulm, Germany; Karlsruhe Institute of Technology (KIT), 76021 Karlsruhe, Germany;* orcid.org/0000-0002-6606-5304; Email: stefano.passerini@kit.edu

Dominic Bresser − *Helmholtz Institute Ulm (HIU), 89081 Ulm, Germany; Karlsruhe Institute of Technology (KIT), 76021 Karlsruhe, Germany;* orcid.org/0000-0001-6429-6048; Email: dominic.bresser@kit.edu

Authors

Alexander Mayer − *Helmholtz Institute Ulm (HIU), 89081 Ulm, Germany; Karlsruhe Institute of Technology (KIT), 76021 Karlsruhe, Germany*

Alessandro Mariani − *Department of Science and Engineering of Materials, Environment, and Urban Planning (SIMAU), Università Politecnica delle Marche, 60131 Ancona, Italy;* orcid.org/0000-0002-3686-2169

Xu Dong − *Helmholtz Institute Ulm (HIU), 89081 Ulm, Germany; Karlsruhe Institute of Technology (KIT), 76021 Karlsruhe, Germany*

Grégoire Vansse − *Helmholtz Institute Ulm (HIU), 89081 Ulm, Germany; Karlsruhe Institute of Technology (KIT), 76021 Karlsruhe, Germany; Univ. Grenoble Alpes, Univ.*

Savoie Mont Blanc, CNRS, Grenoble INP, LEPMI, UMR5279, 38000 Grenoble, France

Patrick Theato − *Karlsruhe Institute of Technology (KIT), Institute for Chemical Technology and Polymer Chemistry, 76131 Karlsruhe, Germany;* orcid.org/0000-0002-4562-9254

Cristina Iojoiu − *Univ. Grenoble Alpes, Univ. Savoie Mont Blanc, CNRS, Grenoble INP, LEPMI, UMR5279, 38000 Grenoble, France; Réseau sur le Stockage Electrochimique de l'Energie (RS2E), CNRS FR3459, 80039 Amiens, France*

Author Contributions

The manuscript was written through contributions of all authors. All authors have given approval to the final version of the manuscript.

Funding

The authors would like to thank the Federal Ministry for Education and Research (BMBF) for financial support within the FestBatt (03XP0175B and 03XP0175C) and the FB2-Poly (03XP0429B and 03XP0429C) project. Financial support from the Helmholtz Association is also kindly acknowledged. **Notes**

The authors declare no competing financial interest.

ACKNOWLEDGMENTS

The group of Prof. Max von Delius at Ulm University is gratefully acknowledged for the NMR service measurements.

REFERENCES

(1) Yoshino, A. The Birth of the Lithium-Ion Battery. *Angew. Chem., Int. Ed.* **2012**, *51*, 5798−5800.

(2) Liang, Y.; Zhao, C. Z.; Yuan, H.; Chen, Y.; Zhang, W.; Huang, J. Q.; Yu, D.; Liu, Y.; Titirici, M. M.; Chueh, Y. L.; Yu, H.; Zhang, Q. A Review of Rechargeable Batteries for Portable Electronic Devices. *InfoMat* **2019**, *1*, 6−32.

(3) Bresser, D.; Hosoi, K.; Howell, D.; Li, H.; Zeisel, H.; Amine, K.; Passerini, S. Perspectives of Automotive Battery R&D in China, Germany, Japan, and the USA. *J. Power Sources* **2018**, *382*, 176−178.

(4) Yang, Z.; Zhang, J.; Kintner-Meyer, M. C. W.; Lu, X.; Choi, D.; Lemmon, J. P.; Liu, J. Electrochemical Energy Storage for Green Grid. *Chem. Rev.* **2011**, *111*, 3577−3613.

(5) Dunn, B.; Kamath, H.; Tarascon, J. M. Electrical Energy Storage for the Grid: A Battery of Choices. *Science* **2011**, *334*, 928−935.

(6) Armand, M.; Axmann, P.; Bresser, D.; Copley, M.; Edström, K.; Ekberg, C.; Guyomard, D.; Lestriez, B.; Novák, P.; Petranikova, M.; Porcher, W.; Trabesinger, S.; Wohlfahrt-Mehrens, M.; Zhang, H. Lithium-Ion Batteries − Current State of the Art and Anticipated Developments. *J. Power Sources* **2020**, *479*, No. 228708.

(7) Tarascon, J. M.; Armand, M. Issues and Challenges Facing Rechargeable Lithium Batteries. *Nature* **2001**, *414*, 359−367.

(8) Tarascon, J. M. Key Challenges in Future Li-Battery Research. *Philos. Trans. R. Soc., A* **2010**, *368*, 3227−3241.

(9) Asenbauer, J.; Eisenmann, T.; Kuenzel, M.; Kazzazi, A.; Chen, Z.; Bresser, D. The Success Story of Graphite as a Lithium-Ion Anode Material-Fundamentals, Remaining Challenges, and Recent Developments Including Silicon (Oxide) Composites. *Sustainable Energy Fuels* **2020**, *4*, 5387−5416.

(10) Xu, W.; Wang, J.; Ding, F.; Chen, X.; Nasybulin, E.; Zhang, Y.; Zhang, J. G. Lithium Metal Anodes for Rechargeable Batteries. *Energy Environ. Sci.* **2014**, *7*, 513−537.

(11) Cheng, X. B.; Zhang, R.; Zhao, C. Z.; Zhang, Q. Toward Safe Lithium Metal Anode in Rechargeable Batteries: A Review. *Chem. Rev.* **2017**, *117*, 10403−10473.

(12) Lin, D.; Liu, Y.; Cui, Y. Reviving the Lithium Metal Anode for High-Energy Batteries. *Nat. Nanotechnol.* **2017**, *12*, 194−206.

(13) Kalhoff, J.; Eshetu, G. G.; Bresser, D.; Passerini, S. Safer Electrolytes for Lithium Ion Batteries: State of the Art and Perspectives. *ChemSusChem* **2015**, *8*, 2154−2175.

(14) He, X.; Bresser, D.; Passerini, S.; Baakes, F.; Krewer, U.; Lopez, J.; Mallia, C. T.; Shao-Horn, Y.; Cekic-Laskovic, I.; Wiemers-Meyer, S.; Soto, F. A.; Ponce, V.; Seminario, J. M.; Balbuena, P. B.; Jia, H.; Xu, W.; Xu, Y.; Wang, C.; Horstmann, B.; Amine, R.; Su, C. C.; Shi, J.; Amine, K.; Winter, M.; Latz, A.; Kostecki, R. The Passivity of Lithium Electrodes in Liquid Electrolytes for Secondary Batteries. *Nat. Rev. Mater.* **2021**, *6*, 1036−1052.

(15) Horstmann, B.; Shi, J.; Amine, R.; Werres, M.; He, X.; Jia, H.; Hausen, F.; Cekic-Laskovic, I.; Wiemers-Meyer, S.; Lopez, J.; Galvez-Aranda, D.; Baakes, F.; Bresser, D.; Su, C. C.; Xu, Y.; Xu, W.; Jakes, P.; Eichel, R. A.; Figgemeier, E.; Krewer, U.; Seminario, J. M.; Balbuena, P. B.; Wang, C.; Passerini, S.; Shao-Horn, Y.; Winter, M.; Amine, K.; Kostecki, R.; Latz, A. Strategies towards Enabling Lithium Metal in Batteries: Interphases and Electrodes. *Energy Environ. Sci.* **2021**, *14*, 5289−5314.

(16) Bresser, D.; Lyonnard, S.; Iojoiu, C.; Picard, L.; Passerini, S. Decoupling Segmental Relaxation and Ionic Conductivity for Lithium-Ion Polymer Electrolytes. *Mol. Syst. Des. Eng.* **2019**, *4*, 779−792.

(17) Di Noto, V.; Lavina, S.; Giffin, G. A.; Negro, E.; Scrosati, B. Polymer Electrolytes: Present, Past and Future. *Electrochim. Acta* **2011**, *57*, 4−13.

(18) Hallinan, D. T., Jr.; Balsara, N. P. Polymer Electrolytes. *Annu. Rev. Mater. Res.* **2013**, *43*, 503−525.

(19) Wang, J.; Li, S.; Zhao, Q.; Song, C.; Xue, Z. Structure Code for Advanced Polymer Electrolyte in Lithium-Ion Batteries. *Adv. Funct. Mater.* **2021**, *31*, 2008208.

(20) Xi, G.; Xiao, M.; Wang, S.; Han, D.; Li, Y.; Meng, Y. Polymer-Based Solid Electrolytes: Material Selection, Design, and Application. *Adv. Funct. Mater.* **2021**, *31*, 2007598.

(21) Bocharova, V.; Sokolov, A. P. Perspectives for Polymer Electrolytes: A View from Fundamentals of Ionic Conductivity. *Macromolecules* **2020**, *53*, 4141−4157.

(22) Mindemark, J.; Lacey, M. J.; Bowden, T.; Brandell, D. Beyond PEO—Alternative Host Materials for Li+-Conducting Solid Polymer Electrolytes. *Prog. Polym. Sci.* **2018**, *81*, 114−143.

(23) Zhang, H.; Li, C.; Piszcz, M.; Coya, E.; Rojo, T.; Rodriguez-Martinez, L. M.; Armand, M.; Zhou, Z. Single Lithium-Ion Conducting Solid Polymer Electrolytes: Advances and Perspectives. *Chem. Soc. Rev.* **2017**, *46*, 797−815.

(24) Mayer, A.; Steinle, D.; Passerini, S.; Bresser, D. Block Copolymers as (Single-Ion Conducting) Lithium Battery Electrolytes. *Nanotechnology* **2022**, *33*, No. 062002.

(25) Strauss, E.; Menkin, S.; Golodnitsky, D. On the Way to High-Conductivity Single Lithium-Ion Conductors. *J. Solid State Electrochem.* **2017**, *21*, 1879−1905.

(26) Kim, H.-K.; Srinivasan, V. Status and Targets for Polymer-Based Solid-State Batteries for Electric Vehicle Applications. *J. Electrochem. Soc.* **2020**, *167*, 130520.

(27) Nguyen, H. D.; Kim, G. T.; Shi, J.; Paillard, E.; Judeinstein, P.; Lyonnard, S.; Bresser, D.; Iojoiu, C. Nanostructured Multi-Block Copolymer Single-Ion Conductors for Safer High-Performance Lithium Batteries. *Energy Environ. Sci.* **2018**, *11*, 3298−3309.

(28) Chen, Z.; Steinle, D.; Nguyen, H. D.; Kim, J. K.; Mayer, A.; Shi, J.; Paillard, E.; Iojoiu, C.; Passerini, S.; Bresser, D. High-Energy Lithium Batteries Based on Single-Ion Conducting Polymer Electrolytes and $Li[Ni_{0.8}Co_{0.1}Mn_{0.1}]O_2$ Cathodes. *Nano Energy* **2020**, *77*, No. 105129.

(29) Steinle, D.; Chen, Z.; Nguyen, H. D.; Kuenzel, M.; Iojoiu, C.; Passerini, S.; Bresser, D. Single-Ion Conducting Polymer Electrolyte for Li||$LiNi_{0.6}Mn_{0.2}Co_{0.2}O_2$ Batteries—Impact of the Anodic Cutoff Voltage and Ambient Temperature. *J. Solid State Electrochem.* **2022**, *26*, 97−102.

(30) Mayer, A.; Nguyen, H.-D.; Mariani, A.; Diemant, T.; Lyonnard, S.; Iojoiu, C.; Passerini, S.; Bresser, D. Influence of Polymer Backbone Fluorination on the Electrochemical Behavior of Single-Ion Conducting Multiblock Copolymer Electrolytes. *ACS Macro Lett.* **2022**, *11*, 982−990.
(31) Mayer, A.; Ates, T.; Varzi, A.; Passerini, S.; Bresser, D. Novel Sulfur-Doped Single-Ion Conducting Multi-Block Copolymer Electrolyte. *Front. Chem.* **2022**, *10*, No. 974202.
(32) Assumma, L.; Nguyen, H. D.; Iojoiu, C.; Lyonnard, S.; Mercier, R.; Espuche, E. Effects of Block Length and Membrane Processing Conditions on the Morphology and Properties of Perfluorosulfonated Poly(Arylene Ether Sulfone) Multiblock Copolymer Membranes for PEMFC. *ACS Appl. Mater. Interfaces* **2015**, *7*, 13808−13820.
(33) Assumma, L.; Iojoiu, C.; Mercier, R.; Lyonnard, S.; Nguyen, H. D.; Planes, E. Synthesis of Partially Fluorinated Poly(Arylene Ether Sulfone) Multiblock Copolymers Bearing Perfluorosulfonic Functions. *J. Polym. Sci., Part A: Polym. Chem.* **2015**, *53*, 1941−1956.
(34) Evans, J.; Vincent, C. A.; Bruce, P. G. Electrochemical Measurement of Transference Numbers in Polymer Electrolytes. *Polymer* **1987**, *28*, 2324−2328.
(35) Zhao, J.; Wang, L.; He, X.; Wan, C.; Jiang, C. Determination of Lithium-Ion Transference Numbers in $LiPF_6$−PC Solutions Based on Electrochemical Polarization and NMR Measurements. *J. Electrochem. Soc.* **2008**, *155*, A292.
(36) Zugmann, S.; Fleischmann, M.; Amereller, M.; Gschwind, R. M.; Wiemhöfer, H. D.; Gores, H. J. Measurement of Transference Numbers for Lithium Ion Electrolytes via Four Different Methods, a Comparative Study. *Electrochim. Acta* **2011**, *56*, 3926−3933.
(37) Frisch, M. J.; Trucks, G. W.; Schlegel, H. B.; Scuseria, G. E.; Robb, M. A.; Cheeseman, J. R.; Scalmani, G.; Barone, V.; Petersson, G. A.; Nakatsuji, H.; Li, X.; Caricato, M.; Marenich, A.; Bloino, J.; Janesko, B. G.; Gomperts, R.; Mennucci, B.; Hratchian, H. P.; Ort, J. V.; Fox, D. J. *Gaussian 09, Revision D.01*; Gaussian, Inc.: Wallingford CT, 2009.
(38) Hanwell, M. D.; Curtis, D. E.; Lonie, D. C.; Vandermeersch, T.; Zurek, E.; Hutchison, G. R. Avogadro: An Advanced Semantic Chemical Editor, Visualization, and Analysis Platform. *Aust. J. Chem.* **2012**, *4*, 17.
(39) Ramette, R. W. Outmoded Terminology: The Normal Hydrogen Electrode. *J. Chem. Educ.* **1987**, *64*, 885.
(40) Trasatti, S. The Absolute Electrode Potential: An Explanatory Note (Recommendations 1986). *Pure Appl. Chem.* **1986**, *58*, 955−966.
(41) Davis, A. P.; Fry, A. J. Experimental and Computed Absolute Redox Potentials of Polycyclic Aromatic Hydrocarbons Are Highly Linearly Correlated over a Wide Range of Structures and Potentials. *J. Phys. Chem. A* **2010**, *114*, 12299−12304.
(42) Méndez-Hernández, D. D.; Tarakeshwar, P.; Gust, D.; Moore, T. A.; Moore, A. L.; Mujica, V. Simple and Accurate Correlation of Experimental Redox Potentials and DFT-Calculated HOMO/LUMO Energies of Polycyclic Aromatic Hydrocarbons. *J. Mol. Model.* **2013**, *19*, 2845−2848.
(43) Abraham, A.; Chakraborty, P. A Review on Sources and Health Impacts of Bisphenol A. *Rev. Environ. Health* **2020**, *35*, 201−210.
(44) Eladak, S.; Grisin, T.; Moison, D.; Guerquin, M.-J.; N'Tumba-Byn, T.; Pozzi-Gaudin, S.; Benachi, A.; Livera, G.; Rouiller-Fabre, V.; Habert, R. A New Chapter in the Bisphenol a Story: Bisphenol S and Bisphenol F Are Not Safe Alternatives to This Compound. *Fertil. Steril.* **2015**, *103*, 11−21.
(45) Noonan, G. O.; Ackerman, L. K.; Begley, T. H. Concentration of Bisphenol a in Highly Consumed Canned Foods on the U. S. Market. *J. Agric. Food Chem.* **2011**, *59*, 7178−7185.
(46) Björnsdotter, M. K.; de Boer, J.; Ballesteros-Gómez, A. Bisphenol A and Replacements in Thermal Paper: A Review. *Chemosphere* **2017**, *182*, 691−706.
(47) Danyliv, O.; Gueneau, C.; Iojoiu, C.; Cointeaux, L.; Thiam, A.; Lyonnard, S.; Sanchez, J. Y. Polyaromatic Ionomers with a Highly Hydrophobic Backbone and Perfluorosulfonic Acids for PEMFC. *Electrochim. Acta* **2016**, *214*, 182−191.
(48) Shaw, H.; Perlmutter, H. D.; Gu, C.; Arco, S. D.; Quibuyen, T. O. Free-Radical Bromination of Selected Organic Compounds in Water. *J. Org. Chem.* **1997**, *62*, 236−237.
(49) Sanchez, E. I.; Fumarola, M. J. N-Bromosaccharin: Benzylic and α-Carbonylic Bromination. *J. Org. Chem.* **1982**, *47*, 1588−1590.
(50) Chen, Y.; Li, K.; Liu, X.; Zhu, J.; Chen, B. Synthesis of Multisubstituted Indenes via Iron-Catalyzed Domino Reaction of Benzylic Compounds and Alkynes. *Synlett* **2013**, *24*, 130−134.
(51) Ratner, M. A.; Shriver, D. F. Ion Transport in Solvent-Free Polymers. *Chem. Rev.* **1988**, *88*, 109−124.
(52) Ratner, M. A.; Johansson, P.; Shriver, D. F. Polymer Electrolytes: Ionic Transport Mechanisms and Relaxation Coupling. *MRS Bull.* **2000**, *25*, 31−37.
(53) Bouchet, R.; Maria, S.; Meziane, R.; Aboulaich, A.; Lienafa, L.; Bonnet, J.-P.; Phan, T. N. T.; Bertin, D.; Gigmes, D.; Devaux, D.; Denoyel, R.; Armand, M. Single-Ion BAB Triblock Copolymers as Highly Efficient Electrolytes for Lithium-Metal Batteries. *Nat. Mater.* **2013**, *12*, 452−457.
(54) Liang, H. P.; Zarrabeitia, M.; Chen, Z.; Jovanovic, S.; Merz, S.; Granwehr, J.; Passerini, S.; Bresser, D. Polysiloxane-Based Single-Ion Conducting Polymer Blend Electrolyte Comprising Small-Molecule Organic Carbonates for High-Energy and High-Power Lithium-Metal Batteries. *Adv. Energy Mater.* **2022**, *12*, 2200013.
(55) Yamada, Y.; Takazawa, Y.; Miyazaki, K.; Abe, T. Electrochemical Lithium Intercalation into Graphite in Dimethyl Sulfoxide-Based Electrolytes: Effect of Solvation Structure of Lithium Ion. *J. Phys. Chem. C* **2010**, *114*, 11680−11685.
(56) Zhang, X.; Kostecki, R.; Richardson, T. J.; Pugh, J. K.; Ross, P. N. Electrochemical and Infrared Studies of the Reduction of Organic Carbonates. *J. Electrochem. Soc.* **2001**, *148*, A1341.